Sulfur record of rising and falling marine oxygen and sulfate levels during the Lomagundi event

Noah J. Planavsky[a,1], Andrey Bekker[b], Axel Hofmann[c], Jeremy D. Owens[a], and Timothy W. Lyons[a]

[a]Department of Earth Sciences, University of California, Riverside, CA 92521; [b]Department of Geological Sciences, University of Manitoba, Winnipeg, MB, Canada R3T 2N2; and [c]Department of Geology, University of Johannesburg, Auckland Park 2006, South Africa

Edited by Andrew H. Knoll, Harvard University, Cambridge, MA, and approved August 30, 2012 (received for review December 9, 2011)

Carbonates from approximately 2.3–2.1 billion years ago show markedly positive $\delta^{13}C$ values commonly reaching and sometimes exceeding +10‰. Traditional interpretation of these positive $\delta^{13}C$ values favors greatly enhanced organic carbon burial on a global scale, although other researchers have invoked widespread methanogenesis within the sediments. To resolve between these competing models and, more generally, among the mechanisms behind Earth's most dramatic carbon isotope event, we obtained coupled stable isotope data for carbonate carbon and carbonate-associated sulfate (CAS). CAS from the Lomagundi interval shows a narrow range of $\delta^{34}S$ values and concentrations much like those of Phanerozoic and modern marine carbonate rocks. The $\delta^{34}S$ values are a close match to those of coeval sulfate evaporites and likely reflect seawater composition. These observations are inconsistent with the idea of diagenetic carbonate formation in the methanic zone. Toward the end of the carbon isotope excursion there is an increase in the $\delta^{34}S$ values of CAS. We propose that these trends in C and S isotope values track the isotopic evolution of seawater sulfate and reflect an increase in pyrite burial and a crash in the marine sulfate reservoir during ocean deoxygenation in the waning stages of the positive carbon isotope excursion.

Lomagundi excursion | Great Oxidation Event | Precambrian

Fluctuations in organic carbon (OC) burial on geological time scales control the redox state of the ocean–atmosphere system and are linked with major geochemical and biological evolutionary events (1, 2). Carbon isotopes in marine carbonate rocks (limestones and dolostones) are generally assumed to track the balance between OC burial and weathering and are therefore the most widely used proxy for carbon cycling through time (3). Isotopic variations recorded in carbonates throughout Earth's history are typically small ($|\delta^{13}C| = 5‰$) and short-lived [<20 million years (Myr)], a pattern attributed to the overall stability of the Earth's biogeochemical carbon cycle (3). However, a significant deviation from this pattern occurred *ca.* 2.3–2.1 billion years (Ga) ago following the initial rise of atmospheric oxygen. Carbonates of this age have markedly positive $\delta^{13}C$ values often reaching +10‰ and peaking above +20‰ (4–8). These markedly positive values—found in over 15 formations worldwide—are traditionally assumed to track the marine dissolved inorganic carbon (DIC) reservoir and to reflect greatly enhanced organic carbon burial (4–8). It has been estimated that 12–22 times the present atmospheric inventory of oxygen was released because of organic carbon burial during this event, commonly referred to as the Lomagundi excursion (LE) (5).

Alternatively, some researchers have attributed the positive $\delta^{13}C$ values of Lomagundi-age carbonates to widespread diagenetic carbonate formation—that is, precipitation below the sediment–water interface (e.g., 9, 10). Models suggesting a diagenetic origin for isotopically heavy carbonates often invoke precipitation in the methanic zone of the sediment column to explain the dramatic ^{13}C enrichments. Methanogenesis occurs once energetically more favorable oxidants (e.g., nitrate, Fe and Mn oxides, and sulfate) are exhausted (11). The net result of methanogenesis is a pore-water DIC reservoir with strongly positive isotope values, provided the isotopically depleted methane is not reoxidized back to DIC (12). Although carbonates formed in the methanic zone can have $\delta^{13}C$ values larger than +10‰ (13–15), similar to those formed during the LE, carbonates with extreme ^{13}C enrichments are rare in shallow-water settings and are typically found adjacent to carbonates with highly negative carbon isotope values linked to local methane oxidation (e.g., 16).

It is possible that the predominance of positive $\delta^{13}C$ values seen in carbonate rocks deposited during the LE reflect an unmatched period of methanogenesis close to the sediment–water interface, and a coupling with Earth's redox evolution could explain the historical uniqueness of the event. Specifically, the LE might be a product of progressive oxygenation of the oceans in phase with the initial rise of atmospheric oxygen and with a concomitant shift in the primary locus of biological methanogenesis from the water column to the surface sediments where carbonate minerals then precipitated with the unique ^{13}C enrichments (9). The coincidence between the onset of the carbon isotope excursion and the initial rise of atmospheric oxygen could be consistent with such a model (17). In this case, the LE would reflect a transition in the ocean from a predominantly anoxic to an oxic redox state, at which point extensive methanogenesis occurred near the sediment–water interface, rather than in the water column, and drove carbonate precipitation. Such conditions would have been favored if sulfate concentrations in seawater were still very low.

Contrasting models for the LE that pit diagenetic controls against isotopic shifts in the oceanic DIC pool (tied to organic carbon burial) have profoundly different implications for the chemistry of the oceans, biogeochemical cycling of carbon, and our basic understanding of Precambrian redox history. Because carbon and sulfur cycles are intricately linked on both global and local scales (18), sulfur isotope records of seawater and pore-water sulfate can be used to test between these two models. The $\delta^{34}S$ values of pore-water sulfate typically increase with depth in sediments due to biological fractionations that favor light sulfur isotopes during bacterial sulfate reduction (BSR). Carbon isotope values of DIC show an initial decrease with depth linked to remineralization of ^{12}C-enriched organic matter with a variety of oxidants (oxygen, Mn^{4+}, Fe^{3+}, nitrate, and sulfate) and then shift to markedly positive values in the methanic zone, where ^{12}C from organic matter is preferentially incorporated into methane (19). Sulfate is structurally substituted into the carbonate lattice during carbonate precipitation (20), and therefore carbonate-associated sulfate (CAS) incorporated during precipitation in the methanic zone should have extremely positive $\delta^{34}S$ values. Further, because sulfate must be essentially depleted before the onset of appreciable methanogenesis, CAS concentrations in

Author contributions: N.J.P., A.B., A.H., J.D.O., and T.W.L. designed research; N.J.P., A.B., A.H. and J.D.O. performed research; N.J.P. and A.B. analyzed data; and N.J.P. wrote the paper.

The authors declare no conflict of interest.

This article is a PNAS Direct Submission.

[1]To whom correspondence should be addressed. E-mail: planavsky@gmail.com.

This article contains supporting information online at www.pnas.org/lookup/suppl/doi:10.1073/pnas.1120387109/-/DCSupplemental.

methanic carbonates should be very low. We would expect subsequent additional diagenetic overprints, such as meteoric recrystallization, to result in lower, rather than higher, CAS concentrations (e.g., 21).

Within this framework, we present a global survey of new, coupled carbonate-carbon and CAS-sulfur isotope data (i.e., from the same sample) from several Lomagundi-age successions. Beyond this general survey, we have focused in greater detail on the Mcheka Formation of the Lomagundi Group, Zimbabwe; the Nash Fork Formation in Wyoming, United States; and the Lower Albanel Formation in Quebec, Canada. Collectively, these formations span the time interval from the peak to the aftermath of the LE and therefore are particularly well-suited to explore the mechanisms responsible for the termination of the event. Importantly, our data are inconsistent with the idea of carbonate precipitation in the methanic zone as the mechanism behind the unparalleled occurrence of long-lived, highly positive $\delta^{13}C$ excursion. By default, the onus is put back on organic carbon burial. Accepting that, the LE challenges us to unravel how the marine system sustained unusually high levels of organic carbon burial at the dawn of atmospheric oxygenation.

Materials

We present results from the Lower Albanel, Kona, Lucknow, Silverton, Nash Fork, and Mcheka formations deposited from approximately 2.2 Ga to approximately 2.05 Ga on the Superior, Kaapvaal, Wyoming, and Zimbabwe cratons. The sedimentology, carbon isotope systematics, age constraints, and tectonic setting of the sampled formations have been described previously (4, 22–25). All of the formations were deposited on broad, carbonate platforms and are composed predominantly of fine-grained (micritic) carbonates, but stromatolites and granular units are locally abundant. Similar to other CAS studies (e.g., 26), we have focused on micrite-rich lithologies. Unfortunately, there are no high-resolution age constraints for the units we sampled within a continuous stratigraphic context (Nash Fork, Kona, Mcheka formations), and so it is difficult to estimate their average sedimentation rates with confidence. We therefore estimated average sedimentation rates following the approach of Kah et al. (27). To be conservative in our estimates, we used a very broad range (40–250 m Myr^{-1}). This range is typical of the postcompaction depositional rates over million-year time scales for better constrained Phanerozoic carbonate platform environments (28, 29).

Results

CAS concentrations in carbonates deposited during the LE are higher than those of typical Precambrian carbonates outside the excursion. All our samples from strata deposited during the excursion yield an average CAS concentration of 150 ppm (±145 ppm, 1 SD). Samples from the Mcheka Formation have an average of 117 ppm (107 ppm, 1 SD), with the uppermost samples typically showing lower concentrations. The Lucknow and Nash Fork formations yield averages of 227 ppm (137 ppm, 1 SD) and 232 ppm (198 ppm, 1 SD), respectively. Carbonates deposited during the final stage of the LE with $\delta^{13}C \leq 5‰$ in the Mistassini Basin, Quebec, show lower CAS concentrations compared to those deposited during the peak of the excursion (with an average of 46 ppm; ±14 ppm, 1 SD). Similarly, Lomagundi CAS concentrations are higher than those typical of carbonates (primarily dolomites) deposited during the later Paleoproterozoic (30, 31), Mesoproterozoic (30, 31), and Neoproterozoic (32) at times when the seawater sulfate reservoir was significantly smaller than that of modern and Phanerozoic oceans (32). Lomagundi CAS concentrations are comparable to those of Paleozoic micritic carbonates (*SI Text*) (33). The inference, then, is that CAS concentrations in Lomagundi-age carbonates fall in the range of typical marine carbonates that precipitated from waters with a significant sulfate concentration.

CAS from each of the studied formations shows a relatively narrow range of typical marine $\delta^{34}S$ values (Fig. 1). Combined, CAS from the six formations yields $\delta^{34}S$ values ranging from +6 to +29‰ (mean + 14‰, $n = 105$). These values closely match those from coeval sulfate evaporites (Fig. 1). In the Mcheka

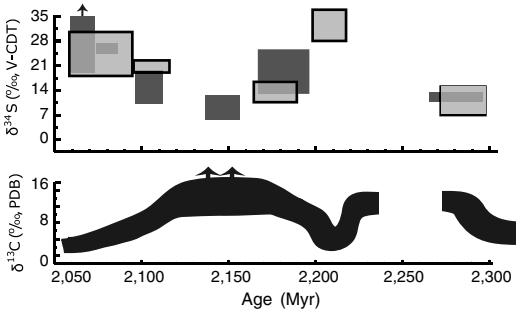

Fig. 1. A generalized $\delta^{13}C_{carbonate}$ trend and available sulfate $\delta^{34}S$ values for the *ca.* 2.3–2.05-Ga time interval. Light-grey boxes are $\delta^{34}S$ values for sulfate evaporite (gypsum and anhydrite), and dark-grey boxes are $\delta^{34}S_{CAS}$ data from this study. Note that $\delta^{34}S_{CAS}$ values are essentially the same as those of coeval sulfate evaporites, suggesting that they record the seawater sulfur isotope composition. There is an antithetic relationship between carbonate $\delta^{13}C$ and sulfate $\delta^{34}S$ values, which is particularly prominent on the falling limb of the Lomagundi carbon isotope excursion (*SI Text* for additional figure information).

Formation, the falling limb of the $\delta^{13}C$ excursion is marked by a systematic upsection increase in $\delta^{34}S_{CAS}$ values (Figs. 2 and 3*A*). There is also an inverse $\delta^{13}C_{carb}$–$\delta^{34}S_{CAS}$ relationship in the Nash Fork Formation, although it is less well-developed. $\delta^{34}S_{CAS}$ values from carbonates of the Mistassini Basin, deposited during the final stages of the Lomagundi excursion (averaging 29‰, maximum 31‰), and in its aftermath (averaging 33‰, maximum 47‰), are higher than those typical of the LE. These results are consistent with the general trend we see for the event: more positive $\delta^{34}S$ values with decreasing $\delta^{13}C$ values.

Diagenetic Influence on Carbonate Precipitation

A coupled C–S isotope approach can be used to test for a diagenetic influence on carbonate precipitation. Sulfate is structurally substituted into the carbonate lattice during carbonate precipitation, and the concentration of CAS is proportional to ambient sulfate concentrations during carbonate precipitation (20, 34). How CAS concentration specifically scales with seawater sulfate concentration is not well-known and can be influenced by a number of factors (e.g., temperature, mineralogy, and crystal growth rate). Additionally, vital effects can also be important in biogenic phases. However, initial CAS concentrations do, in a more straightforward way, scale with seawater concentrations when abiotic precipitation dominates, as in the case with the samples for this study. Diagenesis can change primary CAS concentrations (21), and the effects of dolomitization on CAS are poorly constrained (35). Nevertheless, although CAS concentrations

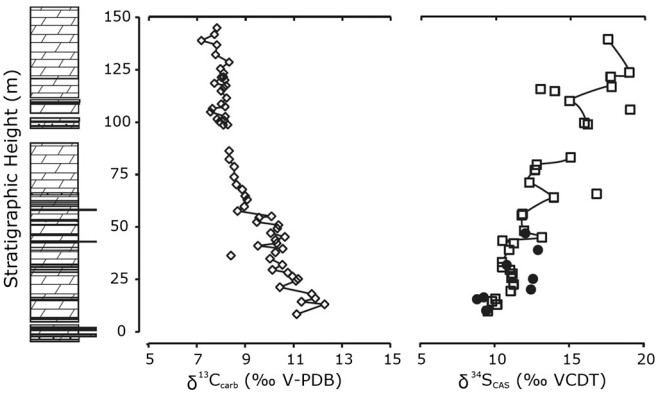

Fig. 2. Carbonate $\delta^{13}C$ and $\delta^{34}S_{CAS}$ stratigraphic trends in the Mcheka Formation, Zimbabwe. The black circles on the $\delta^{34}S_{CAS}$ plot are for a duplicate section approximately 200 m along the strike. $\delta^{34}S_{CAS}$ values systematically increase as carbonate $\delta^{13}C$ values systematically decrease up-section in the Mcheka Formation.

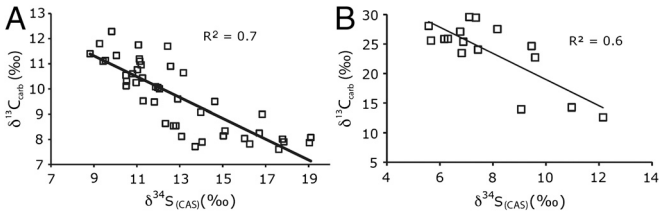

Fig. 3. Carbonate $\delta^{13}C$ and $\delta^{34}S_{CAS}$ cross-plots for (*A*) the Mcheka Formation, Zimbabwe, and (*B*) the Nash Fork Formation, Wyoming, United States.

may shift during diagenesis, they are likely to preserve first-order seawater trends (31). Later diagenetic increases in CAS concentration during recrystallization in the presence of sulfate-rich brines seem unlikely considering that carbonates in our study were collected from different basins, and given the ubiquity of CAS-lean Precambrian calcites and dolomites outside the LE. Therefore, the fact that CAS concentrations in carbonate rocks deposited during the LE fall within the range of typical Phanerozoic marine precipitates (*SI Text*) is noteworthy. Because sulfate should be essentially depleted before the onset of methanogenesis (11), these values are inconsistent with carbonate formation in the methanic zone.

Given that $\delta^{34}S$ values for dissolved sulfate increase with depth in sediments because of fractionations associated with BSR, the very small amounts of CAS, if any, incorporated during precipitation in the methanic zone should have extremely positive $\delta^{34}S$ values associated with the high $\delta^{13}C$ values. In that light, the observed relatively narrow range of moderate $\delta^{34}S_{CAS}$ values from our LE carbonates argues against precipitation in the methanic zone. Furthermore, $\delta^{34}S_{CAS}$ values that closely match those from coeval sulfate evaporites, as we observe, further suggest that our samples record seawater rather than diagenetic C and S isotope signatures (Fig. 3).

Changes in Seawater Sulfate Reservoir Size During the Paleoproterozoic

Our results for CAS concentrations point to a large marine sulfate reservoir during the Lomagundi carbon isotope excursion. It has been demonstrated that the extent of temporal isotopic variability in seawater sulfate across Phanerozoic carbon isotope excursions can effectively track the size of the marine sulfate reservoir, and we can employ the same modeling approach here (36). More specifically, sulfate is buffered against isotopic change when the seawater sulfate reservoir is large and sulfate residence time in the ocean is long. The range of isotopic variability in the Mcheka Formation across the wide range of possible sedimentation rates we assumed for its deposition (see above) is less than or equivalent to those observed during Paleozoic positive carbon isotope excursions (36). Similarly, there is extremely muted (<3‰) $\delta^{34}S_{CAS}$ variability in over 300 m of section from the Kona Dolomite. The relatively invariant $\delta^{34}S_{CAS}$ values in LE carbonates and the high CAS concentrations both suggest a large marine sulfate reservoir (Fig. 4). Marine sulfate concentrations were likely <200 μM in the Archean (37), indicating a orders of magnitude increase during the LE to mM levels—comparable to Phanerozoic levels (Fig. 4). However, significantly higher CAS concentrations in carbonates of the Lomagundi interval compared to those found in Mesoproterozoic and Neoproterozoic carbonates (*SI Text*) point to a decrease in the size of the marine sulfate reservoir in the aftermath of the excursion. More precisely, low CAS concentrations in carbonates of the Mistassini Basin deposited at the final stages and immediately after the LE suggest that the drawdown of seawater sulfate occurred at the end of or shortly after the excursion. Again, although diagenesis can shift CAS concentrations, we are confident that the first-order trends are preserved.

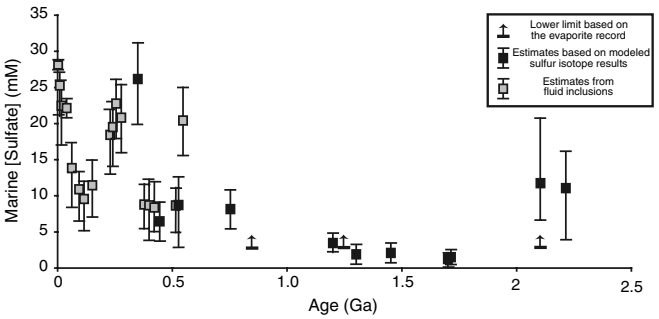

Fig. 4. Estimates of seawater sulfate concentrations through time. Data are from this study and literature sources (*SI Text*). Estimates for Paleoproterozoic sulfate concentrations are based on $\delta^{34}S_{CAS}$ variability for data from the Mcheka Formation (using the approach in ref. 36) and the Kona Dolomite (using the approach in ref. 27).

Our conclusions about the evolution of the marine sulfate reservoir—that is, an increase and then decrease across the LE—are consistent with the available evaporite record. Extensive sulfate deposition during the Lomagundi excursion preceded halite precipitation in the evaporite mineral sequence, as occurs in the Phanerozoic, suggesting that marine sulfate concentrations were higher than approximately 2.5 mM (38). Although 2.5 mM is much less than modern levels (28 mM), this level is within the lowest range of estimates for sulfate concentrations for some intervals of the Phanerozoic (39), and this is a minimum estimate for the LE. Interestingly, this evaporite mineral sequence is not observed in 1.95-Ga rocks (40), where halite precipitated without gypsum, suggesting a return to lower sulfate concentration following the Lomagundi excursion, consistent with low values inferred for the mid-Proterozoic (41). Therefore, the evaporite record also suggests that there was a rise and then fall in the size of the seawater sulfate reservoir in the Paleoproterozoic (Fig. 4).

Sulfur Cycle During the Lomagundi Carbon Isotope Excursion

The observed carbon and sulfur isotope trends indicate a dramatic change in the sulfur cycle during the falling limb of the LE. The inverse stratigraphic relationship for $\delta^{34}S_{CAS}$ and $\delta^{13}C_{carb}$ values in the Mcheka Formation (Figs. 2 and 3), which we assume to be tracking seawater sulfate and DIC, may at first blush seem contradictory because the burial rates of reduced carbon and sulfur are positively coupled in modern marine environments through BSR, which is fueled by organic matter and associated pyrite formation (18). Our understanding of their biogeochemical cycles, however, also allows for the possibility of an inverse isotopic relationship in the sulfate and DIC reservoirs (42–44). Indeed, there is a well-documented antithetic relationship between sulfate $\delta^{34}S$ and carbonate $\delta^{13}C$ values during some long-lived Phanerozoic carbon isotope excursions [e.g., during the Carboniferous (42, 45) and the Phanerozoic, in general, on very long time scales (10^7- to 10^8-year time scales)]. This relationship has been linked to the mass balance between oxidized and reduced C and S compounds (18, 43, 46–48) through the equation:

$$4FeS_2 + 8CaCO_3 + 7MgCO_3 + 7SiO_2 + 31H_2O \leftrightarrow 8CaSO_4 \bullet 2H_2O + 2Fe_2O_3 + 15CH_2O + 7MgSiO_3.$$

This framework has been used to model oxygen levels in the ocean–atmosphere system over Phanerozoic time, and in the simplest sense suggests that the inverse relationship of sulfate $\delta^{34}S$ and carbonate $\delta^{13}C$ is driven by a coupling between the burial of reduced carbon and oxidized sulfur on a global scale. It is, however, difficult to use the same theoretical framework to understand the observed inverse $\delta^{34}S$–$\delta^{13}C$ trends in the

Paleoproterozoic. Isotope mass balance arguments (49) suggest that pyrite dominated the sedimentary sulfur burial flux until the Phanerozoic, when the development of bioturbation significantly changed the global S cycle, and burial of sulfate as gypsum and anhydrite became quantitatively important (49). Therefore, long-term marine sulfate $\delta^{34}S$ isotopic shifts in the Phanerozoic —but not in the Paleoproterozoic—were strongly influenced by changes in the ratio of reduced to oxidized sulfur buried in marine systems.

The observed rise in sulfate $\delta^{34}S$ values and the inverse C–S isotope relationship during the falling limb of the LE can be linked to increased pyrite burial during a global deoxygenation event. Increased pyrite burial, without a corresponding decrease in gypsum burial, at the end of the LE would have triggered a dramatic drop in the size of the marine sulfate reservoir and an increase in the marine sulfate $\delta^{34}S$ value. If the markedly positive carbonate $\delta^{13}C$ values that characterize the LE are linked to enhanced organic carbon burial (cf. 5), it would follow that there would be a drop in the oxygen levels of the ocean–atmosphere system (caused by lower organic carbon burial and a smaller O_2 flux) at the end of the LE. The switch to a more reducing ocean–atmosphere system may also be the consequence of oxidation of uplifted organic carbon-rich rocks buried during the early stages of the LE (50). A global increase in pyrite burial should accompany the switch to a more reducing ocean—because sulfide reoxidation will decrease as marine anoxia becomes more expansive (e.g., 51). Given this framework, the rise in sulfate $\delta^{34}S$ values during the end of the LE reflects a drop in oceanic oxygen levels that promoted enhanced pyrite burial (and thus more burial of isotopically light sulfur). At the core of this model is the requirement that large swaths of the ocean were ventilated during the LE and became less oxygenated in its wake.

The observed inverse C–S relationship between sulfate $\delta^{34}S$ and carbonate $\delta^{13}C$ values in the LE may also be tied to decreases in the extent of continental pyrite oxidation and concomitantly in the magnitude of the continental sulfate flux (52). Limited terrestrial sulfide oxidation in the Archean would have led to higher-than-modern levels of reduced sulfur in the upper crust available for terrestrial weathering (52, 53). With an anoxic atmosphere, the majority of sulfides during weathering would be transported from continental settings to shallow marine environments without being oxidized—leading to burial of detrital pyrites. It has been proposed that first exposure of upper continental crust developed under essentially anoxic conditions to an oxygenated world would fuel intense pyrite oxidation, enhanced sulfate delivery to the oceans, and growth of the marine sulfate reservoir (52, 53). A larger marine sulfate reservoir and a fully oxidative continental sulfur cycle is likely to yield a decrease in the ratio of sulfur buried on the continental margin relative to deep-sea environments. This shift is significant because sediments on the margin have a much higher potential than deep-sea environments to escape subduction and instead be exhumed and subjected to continental weathering. On geologic time scales (tectonic-recycling time scales), increasing deep-sea sulfur burial may result in a decrease in the average amount of sulfide present in exhumed marine sedimentary rocks. The termination of the LE is about one to two sedimentary rock half-lives (somewhere between 100 and 300 Myr—e.g., ref. 54) after the rise of atmospheric oxygen, which is the time required for tectonic processes to replace Archean pyrite-rich sedimentary rocks with the less pyrite-rich sedimentary rocks formed in the wake of the Great Oxidation Event (53). Therefore, it is possible that the sulfur isotope behavior observed at the end of the LE corresponded with a decrease in the continental sulfate flux, which (along with increased pyrite burial) could also drive a shift to more positive sulfate $\delta^{34}S$ values.

This decrease in the amount of sulfide present in the upper crust may also be linked to the anomalous carbonate $\delta^{13}C$ values that characterize the LE (53). Increased pyrite oxidation in continental weathering environments would have increased acid generation, which could have fueled increased apatite dissolution and amplified the continental phosphorus flux to the oceans. A stronger continental phosphate flux would have enhanced organic carbon burial on a global scale, ultimately leading to the shift to positive carbonate $\delta^{13}C$ values (53). High rates of sulfide oxidation would have also increased the flux of some bioessential metals (e.g., molybdenum), which may have been biolimiting up to that point (e.g., 55).

A simple, global S cycle box modeling approach (e.g., 33, 56) can be used to evaluate the relative roles that increased pyrite burial and a decreased continental sulfate flux played in controlling sulfate $\delta^{34}S$ trends during the tail end of the LE (*SI Text* for model description). A strong increase in pyrite burial (approximately two- to threefold increase from the global modern pyrite burial flux) is needed to reproduce the observed shift in $\delta^{34}S$ values at the end of the LE (*SI Text*). This shift in burial is equivalent to estimates for increased burial during Phanerozoic ocean anoxic events (OAEs) (e.g., 33), suggesting relatively dramatic shifts in sulfur burial and the global redox landscape during the end of the LE. Given a reasonable set of model parameters (*SI Text*), it is not possible to drive the rise in sulfate $\delta^{34}S$ values observed at the tail end of the LE exclusively through decreases in the continental sulfate flux. However, it is possible to reproduce the observed trend via a decrease from 115% to 100% of the modern continental sulfate input, as long as there is also a correspondingly strong (three- to fourfold) increase in the amount of marine pyrite burial. Use of much higher continental sulfate inputs (e.g., 130% of modern) results in unrealistically high sulfate concentrations or requires unreasonable pyrite burial fluxes and fractionation factors (*SI Text*). Implicit in this modeling approach is that pyrite dominated the marine S burial flux in the Paleoproterozoic (cf. 49). A key question is if an approximately 10% to 20% increase in the amount of weathering-mediated pyrite oxidation during the peak of the LE would be able to alter significantly the continental phosphorus flux and drive enhanced organic carbon burial (53).

Conclusions

Approximately 2.3- to 2.1-Ga carbonate rocks have markedly positive $\delta^{13}C$ values, commonly reaching beyond $+10‰$. Because C and S isotopes of dissolved inorganic carbon and sulfate follow predictable trends in diagenetic settings, we can use these isotopic systems to identify or rule out diagenetic carbonate precipitation. Specifically, sulfate $\delta^{34}S$ values increase with burial depth because of biological fractionations associated with BSR, whereas DIC isotope values show an initial decrease followed by a shift to markedly positive values in the methanic zone (16). In contrast to the trend predicted for early diagenesis, we found a narrow range of moderate S isotope values in each of the studied carbonate units deposited between approximately 2.3 and 2.1 Ga that is essentially the same as that of the coeval sulfate evaporites, which is inconsistent with carbonate formation in the methanic zone. Lomagundi-excursion carbonates appear to record seawater C and S isotope signatures, and can thus contribute to our understanding of Paleoproterozoic biogeochemical cycles.

High [CAS] and relatively low variability of CAS $\delta^{34}S$ values in LE carbonates relative to younger Proterozoic equivalents point to a large coeval marine sulfate reservoir followed by a decrease in seawater concentrations. The falling limb of the Lomagundi excursion is marked by an increase in $\delta^{34}S_{CAS}$ and a strong decrease in [CAS]. We propose that these changes reflect an increase in pyrite burial and a crash in the marine sulfate reservoir during ocean deoxygenation in the waning stages of the positive carbon isotope excursion. A simple global mass balance model for sulfur suggests that there was at least a two- to threefold increase in global pyrite burial at the end of the LE—equiva-

lent to the magnitude of increases associated with the Phanerozoic OAEs. This large shift in pyrite burial suggests the end of the LE was marked by a significant redox shift and points toward a dramatic rise and fall in oxygen levels in the ocean atmosphere system during the Paleoproterozoic. It seems likely that deoxygenation of the ocean–atmosphere system at the end of the LE was an inevitable consequence of decreased organic carbon burial and parallel O_2 loss via oxidation of exhumed organic carbon-rich sediments buried during the peak of the LE. There is mounting evidence that, in contrast to the traditional view of a unidirectional oxygen rise, there was significant variability in the redox state of Earth's surface during the Precambrian (50, 53).

Methods

We used a CAS extraction method modified from traditional approaches to ensure that sulfide oxidation during extraction is negligible. In summary, 20 to 100 g of powder was exposed to successive NaCl and H_2O_2 treatments with two distilled-water rinses following each step. The intent is to remove sulfates and sulfides (foremost HCl-soluble iron monosulfides) that might skew the primary CAS record. The powders were then dissolved through slow addition of a 5% $SnCl_2$ 4N HCl solution. Addition of $SnCl_2$, a reductant, prevented sulfide oxidation by reaction with any Fe(III) liberated during the HCl addition, thus minimizing contamination to the CAS signal. Liberated primary CAS was precipitated through addition of BaCl to induce barite precipitation. Sulfur isotope measurements were made after on-line barite combustion using a ThermoFinnigan DeltaV Plus continuous-flow stable isotope ratio mass spectrometer at University of California, Riverside. Reproducibility was better than 0.2‰ based on single-run and long-term standard monitoring. CAS concentrations were measured using an Agilent inductively coupled plasmonic MS in the Xe collision-cell mode to reduce oxide interferences, and reproducibility was better than 88%. We estimated Paleoproterozoic sulfate concentrations based on maximum $\delta^{34}S_{CAS}$ variability following the approach in ref. 36 for the Mcheka Formation, and using the approach in ref. 27 for the Kona Dolomite. Error bars reflect the range of estimates for the duration the examined sequences. Global sulfur cycle box modeling was done following the approach in ref. 32. Model parameters and sensitivity tests are presented in refs. 32 and 53 and *SI Text*.

ACKNOWLEDGMENTS. We are grateful to Ben Gill, Bill Gilhooly, Chris Reinhard, and Don Canfield for formative discussions; Galen Halverson and anonymous reviewers for constructive comments; S. Bates for assistance with the analyses; and the Geology Department of the University of Zimbabwe for logistical support. This work was supported by National Science Foundation Graduate Research Fellowship program and American Philosophical Society (N.J.P.); National Science Foundation Division of Earth Sciences and National Aeronautics and Space Administration Exobiology Program (T.W.L.); Natural Sciences and Engineering Research Council of Canada (A.B.); and the National Research Foundation of South Africa (A.H.).

1. Holland HD (1984) *The Chemical Evolution of the Atmosphere and Oceans* (Princeton Univ Press, Princeton) p 598.
2. Schidlowski M (1987) Application of stable carbon isotopes to early biochemical evolution on Earth. *Annu Rev Earth Planet Sci* 15:47–72.
3. Schidlowski M (2001) Carbon isotopes as biogeochemical recorders of life over 3.8 Ga of Earth history: Evolution of a concept. *Precambrian Res* 106:117–134.
4. Bekker A, Karhu JA, Kaufman AJ (2006) Carbon isotope record for the onset of the Lomagundi carbon isotope excursion in the Great Lakes area, North America. *Precambrian Res* 148:145–180.
5. Karhu JA, Holland HD (1996) Carbon isotopes and the rise of atmospheric oxygen. *Geology* 24:867–870.
6. Maheshwari A, et al. (2010) Global nature of the Paleoproterozoic Lomagundi carbon isotope excursion: A review of occurrences in Brazil, India, and Uruguay. *Precambrian Res* 182:274–299.
7. Melezhik VA, Fallick AE (1996) A widespread positive delta C-13(carb) anomaly at around 2.33–2.06 Ga on the Fennoscandian Shield: A paradox? *Terra Nova* 8:141–157.
8. Schidlowski M, Eichmann R, Junge CE (1976) Carbon isotope geochemistry of Precambrian Lomagundi Carbonate Province, Rhodesia. *Geochim Cosmochim Acta* 40:449–455.
9. Hayes JM, Waldbauer JR (2006) The carbon cycle and associated redox processes through time. *Philos Trans R Soc B* 361:931–950.
10. Yudovich YE, Makarikhin VV, Medvedev PV, Sukhanov NV (1991) Carbon isotope anomalies in carbonates of the Karelian Complex. *Geochem Int* 28:56–62.
11. Canfield DE, Kristensen E, Thamdrup B (2005) *Aquatic Geomicrobiology* (Elsevier, Amsterdam).
12. Claypool GE, Kaplan IR (1974) The origin and distribution of methane in marine sediments. *Natural Gases in Marine Sediments*, ed IR Kaplan (Plenum, New York), pp 99–139.
13. Hennessy J, Knauth LP (1985) Isotopic variations in dolomite concretions from the Monterey Formation, California. *J Sediment Petrol* 55:120–130.
14. Irwin H, Curtis C, Coleman M (1977) Isotopic evidence for source of diagenetic carbonates formed during burial of organic-rich sediments. *Nature* 269:209–213.
15. Talbot MR, Kelts K (1986) Primary and diagenetic carbonates in the anoxic sediments of Lake Bosumtwi, Ghana. *Geology* 14:912–916.
16. Maynard JB (1982) Extension of Berner's new geochemical classification of sedimentary environments to ancient sediments. *J Sediment Petrol* 52:1325–1331.
17. Guo QJ, et al. (2009) Reconstructing Earth's surface oxidation across the Archean-Proterozoic transition. *Geology* 37:399–402.
18. Berner RA (1989) Biogeochemical cycles of carbon and sulfur and their effect on atmospheric oxygen over Phanerozoic time. *Global Planet Change* 75:97–122.
19. Böttcher ME (1999) Carbon, sulfur and oxygen isotope geochemistry in interstitial waters from the western Mediterranean. *Proc Ocean Drill Program* 161:413–422.
20. Pingitore NE, Meitzner G, Love KM (1995) Identification of sulfate in natural carbonates by X-ray absorption spectroscopy. *Geochim Cosmochim Acta* 59:2477–2483.
21. Gill BC, Lyons TW, Frank TD (2008) Behavior of carbonate-associated sulfate during meteoric diagenesis and implications for the sulfur isotope paleoproxy. *Geochim Cosmochim Acta* 72:4699–4711.
22. Bekker A, et al. (2008) Fractionation between inorganic and organic carbon during the Lomagundi (2.22–2.1 Ga) carbon isotope excursion. *Earth Planet Sci Lett* 271:278–291.
23. Bekker A, Karhu JA, Eriksson KA, Kaufman AJ (2003) Chemostratigraphy of Paleoproterozoic carbonate successions of the Wyoming Craton: Tectonic forcing of biogeochemical change? *Precambrian Res* 120:279–325.
24. Bekker A, Kaufman AJ, Karhu JA, Eriksson KA (2005) Evidence for Paleoproterozoic cap carbonates in North America. *Precambrian Res* 137:167–206.
25. Master S, Bekker A, Hofmann A (2010) A review of the stratigraphy and geological setting of the Palaeoproterozoic Magondi Supergroup, Zimbabwe—Type locality for the Lomagundi carbon isotope excursion. *Precambrian Res* 182:254–273.
26. Kampschulte A, Strauss H (2004) The sulfur isotopic evolution of Phanerozoic seawater based on the analysis of structurally substituted sulfate in carbonates. *Chem Geol* 204:255–286.
27. Kah LC, Lyons TW, Frank T (2004) Low marine sulphate and protracted oxygenation of the Proterozoic biosphere. *Nature* 431:834–837.
28. Bosscher H, Schlager W (1993) Accumulation rates of carbonate platforms. *J Geol* 101:345–355.
29. McNeill DF (2005) Accumulation rates from well-dated late Neogene carbonate platforms and margins. *Sediment Geol* 175:73–87.
30. Chu XL, Zhang TG, Zhang QR, Lyons TW (2007) Sulfur and carbon isotope records from 1700 to 800 Ma carbonates of the Jixian section, northern China: Implications for secular isotope variations in Proterozoic seawater and relationships to global supercontinental events. *Geochim Cosmochim Acta* 71:4668–4692.
31. Gellatly AM, Lyons TW (2005) Trace sulfate in mid-Proterozoic carbonates and the sulfur isotope record of biospheric evolution. *Geochim Cosmochim Acta* 69:3813–3829.
32. Hurtgen MT, Arthur MA, Halverson GP (2005) Neoproterozoic sulfur isotopes, the evolution of microbial sulfur species, and the burial efficiency of sulfide as sedimentary pyrite. *Geology* 33:41–44.
33. Gill BC, et al. (2011) Geochemical evidence for widespread euxinia in the Later Cambrian ocean. *Nature* 469:80–83.
34. Pavlov AA, Hurtgen MT, Kasting JF, Arthur MA (2003) Methane-rich Proterozoic atmosphere? *Geology* 31:87–90.
35. Staudt WJ, Schoonen MAA (1995) Sulfate incorporation into sedimentary carbonates. *Geochemical Transformations of Sedimentary Sulfur*, eds MA Vairavamurthy and MAA Schoonen (American Chemical Society, Washington, DC), pp 332–345.
36. Gill BC, Lyons TW, Saltzman MR (2007) Parallel, high-resolution carbon and sulfur isotope records of the evolving Paleozoic marine sulfur reservoir. *Palaeogeogr Palaeoclimatol Palaeoecol* 256:156–173.
37. Habicht KS, Gade M, Thamdrup B, Berg P, Canfield DE (2002) Calibration of sulfate levels in the Archean Ocean. *Science* 298:2372–2374.
38. Schröeder S, Bekker A, Beukes NJ, Strauss H, van Niekerk HS (2008) Rise in seawater sulphate concentration associated with the Paleoproterozoic positive carbon isotope excursion: Evidence from sulphate evaporites in the similar to 2.2–2.1 Gyr shallow-marine Lucknow Formation, South Africa. *Terra Nova* 2:108–117.
39. Lowenstein TK, Timofeeff MN, Brennan ST, Hardie LA, Demicco RV (2001) Oscillations in Phanerozoic seawater chemistry: Evidence from fluid inclusions. *Science* 294:1086–1088.
40. Pope MC, Grotzinger JP (2003) Paleoproterozoic Stark Formation, Athapuscow Basin, Northwest Canada: Record of cratonic-scale salinity crisis. *J Sediment Res* 73:280–295.
41. Canfield DE, Farquhar J, Zerkle AL (2010) High isotope fractionations during sulfate reduction in a low-sulfate euxinic ocean analog. *Geology* 38:415–418.
42. Carpenter SJ, Lohmann KC (1997) Carbon isotope ratios of Phanerozoic marine cements: Re-evaluating the global carbon and sulfur systems. *Geochim Cosmochim Acta* 61:4831–4846.
43. Garrels RM, Lerman A (1984) Coupling of the sedimentary sulfur and carbon cycles: An improved model. *Am J Sci* 284:989–1007.
44. Walker JCG (1986) Global geochemical cycles of carbon, sulfur and oxygen. *Mar Geol* 70:159–174.
45. Veizer J, Holser WT, Wilgus CK (1980) Correlation of C-13-C-12 and S-34-S-32 secular variations. *Geochim Cosmochim Acta* 44:579–587.
46. Berner RA, Raiswell R (1983) Burial of organic carbon and pyrite sulfur in sediments over Phanerozoic time: A new theory. *Geochim Cosmochim Acta* 47:855–862.

47. Carpenter SJ, Lohmann KC (1999) Reply to the comment by S. T. Petsch on carbon isotope ratios of Phanerozoic marine cements: Re-evaluating global carbon and sulfur systems. *Geochim Cosmochim Acta* 63:761–766.
48. Kump LR, Garrels RM (1986) Modeling atmospheric O_2 in the global sedimentary redox cycle. *Am J Sci* 286:337–360.
49. Canfield DE, Farquhar J (2009) Animal evolution, bioturbation, and the sulfate concentration of the oceans. *Proc Natl Acad Sci USA* 106:8123–8127.
50. Kump LR, et al. (2011) Isotopic evidence for massive oxidation of organic matter following the Great Oxidation Event. *Science* 334:1694–1696.
51. Canfield DE (1998) A new model for Proterozoic ocean chemistry. *Nature* 396:450–453.
52. Holland HD (2002) Volcanic gases, black smokers, and the Great Oxidation Event. *Geochim Cosmochim Acta* 66:3811–3826.
53. Bekker A, Holland HD (2012) Oxygen overshoot and recovery during the early Paleoproterozoic. *Earth Planet Sci Lett* 317:295–304.
54. Garrels RM, McKenzie F (1971) *Evolution of Sedimentary Rocks* (Norton, New York) p 397.
55. Planavsky NJ, et al. (2010) The evolution of the marine phosphate reservoir. *Nature* 467:1088–1090.
56. Gill BC, Lyons TW, Jenkyns HC (2011) A global perturbation to the sulfur cycle during the Toarcian oceanic anoxic event. *Earth Planet Sci Lett* 312:484–496.

Supporting Information

Planavsky et al. 10.1073/pnas.1120387109

SI Text

Global Sulfur Cycle Model. We used a widely employed global sulfur cycle box modeling approach (e.g., 1–3) to explore the dynamics and significance of the carbonate-associated sulfate (CAS) isotope record at the end of the Lomagundi excursion (LE). Gill et al. (2) and Kurtz et al. (4) recently described the modeling approach in detail, so we only provide an overview. We used the following expression to mimic the isotopic change of the global marine sulfate reservoir:

$$\frac{\partial \delta_0}{\partial t} = \frac{F_W(\delta_W - \delta_0) - F_{py}\Delta S}{M_0}$$

where M_0 and δ_0 are the amount of sulfate S in the ocean reservoir and its isotopic composition, respectively. The input to the ocean, F_W, includes sulfur fluxes to the marine system from weathering and magmatic processes, and is assigned a single, average isotopic composition (δw). F_{py} is the pyrite burial flux and ΔS is the mean fractionation from oceanic sulfate caused by bacterial sulfate reduction and pyrite formation. Consistent with the sulfide $\delta^{34}S$ record (e.g., 5), we have used a lower $\Delta^{34}S$ value than is typically used for Phanerozoic modeling work (Fig. S1), and we have assumed a constant $\Delta^{34}S$ throughout the LE. Initial and nonvarying boundary conditions (Fig. S1) are similar to those used in Phanerozoic sulfur cycle models (e.g., 2). The one exception is that evaporate burial, which does not have a significant associated isotopic fractionation, was held below 15% of the modern flux. Estimates of marine sulfur concentrations, along with the reduced to oxidized sulfur ratio of the marine burial flux during the LE are discussed in the main text. We constructed the model using STELLA™ modeling software and employed a forward modeling approach—varying key boundary conditions for the sulfur cycle (Fig. S2), in order to best recreate the observed sulfur isotopic profile.

We have modeled the observed rise in marine sulfate $\delta^{34}S$ values during the falling limb of the LE. More specifically, we modeled a rise in the $\delta^{34}S$ value of marine sulfate from approximately 13‰ to approximately 28‰ over 50 million years (Myr). The observed isotopic shift may have occurred more rapidly than 50 Myr (estimated to have occurred between 30–50 Myr; Fig. 2). However, given that our conclusion is that this isotope shift represents a significant geochemical perturbation, this long timespan is conservative. We suggest the data are best reproduced with a strong (2.7-fold) increase in pyrite burial (relative to the modern global burial flux), a modern continental sulfate flux, a starting marine sulfate concentration of 7 mM, and mean $\Delta^{34}S$ value of −17‰ transiently increasing to −21‰ (Fig. S1). The sulfate $\delta^{34}S$ values can also be reproduced with an elevated continental sulfate flux. However, with a larger continental sulfate flux, an increase in the global pyrite burial flux is needed to reproduce the rise in $\delta^{34}S$ values at the tail end of the LE. For instance, a 3.2-fold increase in the global pyrite burial flux relative to the modern is needed given a transient decrease from 115% to 100% of the modern continental sulfate flux over the 50-Myr period. Model runs using very elevated continental sulfate fluxes ($\gtrsim$ 120% of the modern flux), without inducing extensive gypsum burial (at least 50% modern evaporate burial), yield very high (>20 mM) marine sulfate concentrations. Marine sulfate concentrations above 20 mM are inconsistent with available estimates for the size of the marine sulfate reservoir in the mid-Paleoproterozoic (see main text).

Sensitivity tests for key model variables are shown in Fig. S2. The model is sensitive enough to pyrite burial (Fig. S2*A*) that the percent increase in pyrite burial can be estimated within a relatively narrow range (an increase in pyrite burial to >2.15 and <3.15 times the modern flux). However, as noted above, if the observed rise in carbonate-associated sulfate (CAS) $\delta^{34}S$ values occurred over a shorter time period than estimated, larger increases in pyrite burial will be needed (Fig. S2*A*). The model is also very sensitive to the magnitude of the continental weathering flux (all other parameters being held constant)—15% changes in the magnitude of the continental sulfate flux lead to large (>5 mM) changes in the peak marine sulfate concentrations (Fig. S2*B*). The starting sulfate concentration makes little difference on the trajectory of the isotopic profile (Fig. S2*C*), but does affect the peak sulfate concentration and the sulfate concentration at the end of the event. In contrast, strong (>10‰) shifts in the ΔS value can significantly decrease (>10 Myr) the time needed to induce the observed isotopic shift, but varying the ΔS value has no effect on the sulfate concentrations (Fig. S2*D*). However, there is not current evidence that global mean pyrite $\delta^{34}S$ values varied substantially throughout the mid-Paleoproterozoic (e.g., 5).

It has been proposed that an increase in hydrothermal activity can cause an antithetic relationship in marine sulfate $\delta^{34}S$ and carbonate $\delta^{13}C$ records, with light $\delta^{34}S$ values being linked to strong mantle-derived sulfur fluxes (6, 7). Although the end of the Lomagundi excursion coincides with the breakup of Kenorland and, likely, enhanced hydrothermal activity, we note that the pattern predicted by this model is opposite from what we observe in the rock record (Fig. 2). A shift to positive carbon isotope values is expected with enhanced hydrothermal activity and downward trend in S isotope values (6, 7). Given this framework, any changes in the hydrothermal S flux during the LE would require more pronounced shifts in pyrite burial at the end of the LE than we have predicted. We have not varied the hydrothermal sulfur flux in the model runs, which renders our conclusions conservative.

1. Garrels RM, Lerman A (1984) Coupling of the sedimentary sulfur and carbon cycles: An improved model. *Am J Sci* 284:989–1007.
2. Gill BC, et al. (2011) Geochemical evidence for widespread euxinia in the Later Cambrian ocean. *Nature* 469:80–83.
3. Kump LR, Garrels RM (1986) Modeling atmospheric O2 in the global sedimentary redox cycle. *Am J Sci* 286:337–360.
4. Kurtz AC, Kump LR, Arthur MA, Zachos JC, Paytan A (2003) Early Cenozoic decoupling of the global carbon and sulfur cycles. *Palaeogeogr Palaeoclimatol Palaeoecol*, 10 .1029/2003PA000908.
5. Canfield DE (2004) The evolution of the Earth surface sulfur reservoir. *Am J Sci* 304:839–861.
6. Carpenter SJ, Lohmann KC (1997) Carbon isotope ratios of Phanerozoic marine cements: Re-evaluating the global carbon and sulfur systems. *Geochim Cosmochim Acta* 61:4831–4846.
7. Walker JCG (1986) Global geochemical cycles of carbon, sulfur and oxygen. *Mar Geol* 70:159–174.

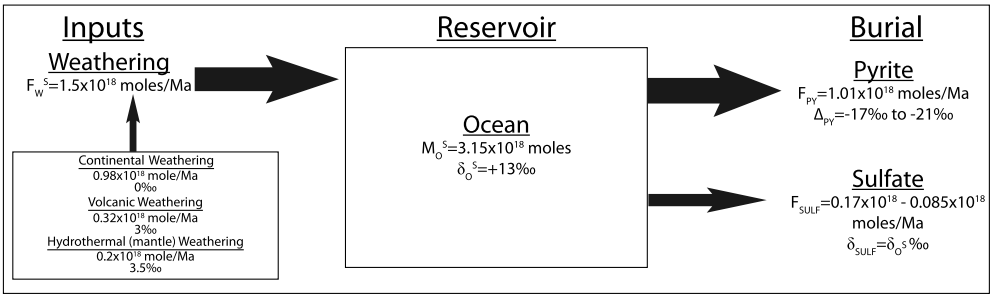

Fig. S1. Overview of utilized global sulfur cycle model parameters.

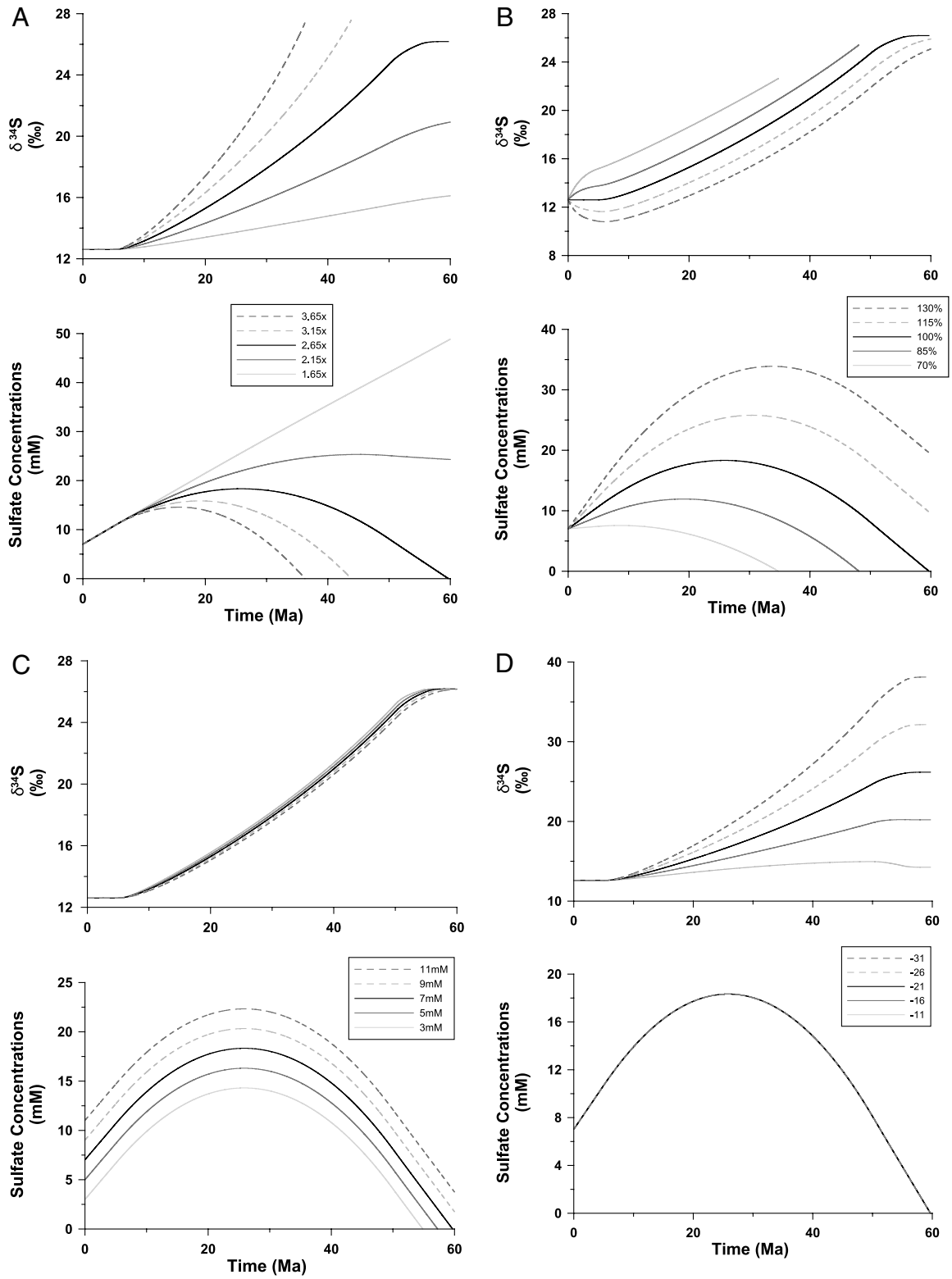

Fig. S2. Sensitivity tests for global S cycle model. We modeled a rise in the $\delta^{34}S$ value of marine sulfate from approximately 13‰ to approximately 28‰ over 50 Myr during the end of the Lomagundi excursion. We suggest the data are best reproduced with a 2.7-fold increase in pyrite burial relative to the global modern burial flux, a modern continental sulfate flux, a starting marine sulfate concentration of 7 mM, and mean $\Delta^{34}S$ value of −17‰ transiently increasing to −21‰. All sensitivity tests (*A*–*D*) use these model parameters. (*A*) Effects of variations in the magnitude of the pyrite burial flux on the trajectory of the $\delta^{34}S$ value rise and on the size of the global marine sulfate reservoir. (*B*) Effects of variations in the magnitude of the continental weathering (sulfate) flux on the trajectory of the $\delta^{34}S$ value rise and on the size of the global marine sulfate reservoir. (*C*) Effects of variations in initial marine sulfate concentrations on the trajectory of the $\delta^{34}S$ value rise and on the size of the global marine sulfate reservoir. (*D*) Effects of variations in pyrite fractionation factors ($\Delta^{34}S$ values) on trajectory of the $\delta^{34}S$ value rise and on the size of the global marine sulfate reservoir.

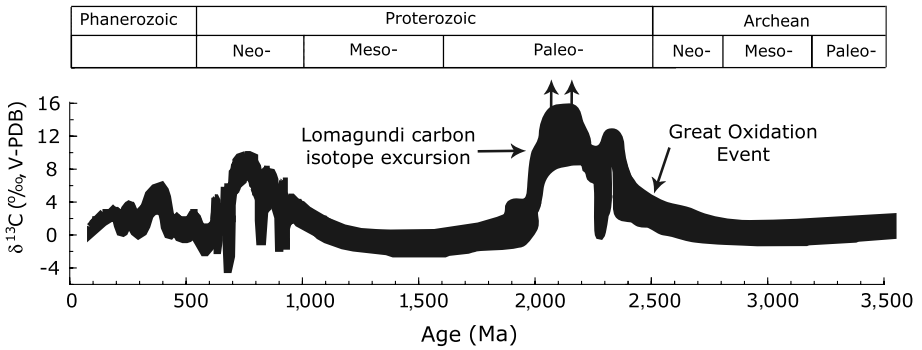

Fig. S3. Generalized carbonate-carbon isotope curve through time. The Lomagundi positive carbon isotope excursion is the longest and largest deviation from the near-zero $\delta^{13}C$ values typical of carbonates throughout Earth's history. The onset of the Lomagundi excursion closely follows the initial rise in atmospheric oxygen (cf. 1). Based on the global pattern of carbon isotope values in Paleoproterozoic marine carbonates, the Lomagundi excursion likely encompassed at least two separate intervals of markedly positive $\delta^{13}C$ values. Modified from ref. 2.

1 Bekker A, et al. (2004) Dating the rise of atmospheric oxygen. *Nature* 427:117.
2 Karhu JA (1999) *Encyclopedia of Geochemistry,* eds Marshall CP, Fairbridge RW (Kluwer Academic Publishers, Boston), pp 67–73.

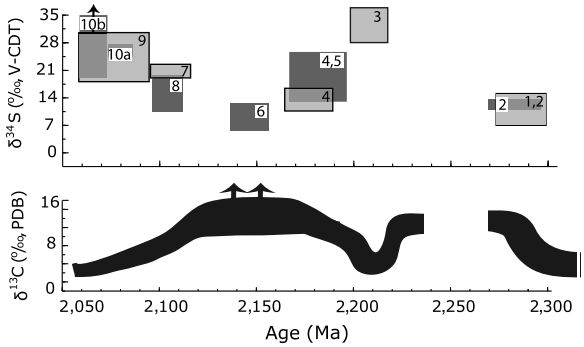

Fig. S4. A generalized $\delta^{13}C_{carbonate}$ trend and available sulfate $\delta^{34}S$ values for the *ca*. 2.3–2.05-billion-year (Ga) time interval. Light-grey boxes are $\delta^{34}S$ values for sulfate evaporite (gypsum and anhydrite), and dark-grey boxes are $\delta^{34}S_{CAS}$ data from this study. The $\delta^{13}C_{carbonate}$ curve is modified from ref. 1, and the compilation of sulfate evaporite S isotope values is from ref. 2 (also presented in Table S4). The $\delta^{34}S_{CAS}$ values are from this study. The ages of the units (and the duration) is based on the available constraints from radiometric ages (see ref. 2) and the carbonate-carbon isotope data, relative to the idealized carbon isotope curve. 1, Gordon Lake Formation; 2, Kona Dolomite; 3, Lower Umba Formation; 4, Lucknow Formation; 5, Silverton Formation; 6, Nash Fork; 7, Delwara Formation and Jhamarkotra Formation; 8, Mcheka Formation; 9, Fedorovka Formation; 10a, Lower Albanel Formation (Lomagundi Excursion); 10b, Lower Albanel Formation (post Lomagundi Excursion)

1 Bekker A, Karhu JA, Kaufman AJ (2006) Carbon isotope record for the onset of the Lomagundi carbon isotope excursion in the Great Lakes area, North America. *Precambrian Res* 148:145–180.
2 Schröeder S, Bekker A, Beukes NJ, Strauss H, van Niekerk HS (2008) Rise in seawater sulphate concentration associated with the Paleoproterozoic positive carbon isotope excursion: Evidence from sulphate evaporites in the similar to 2.2–2.1 Gyr shallow-marine Lucknow Formation, South Africa. *Terra Nova* 2:108–117.

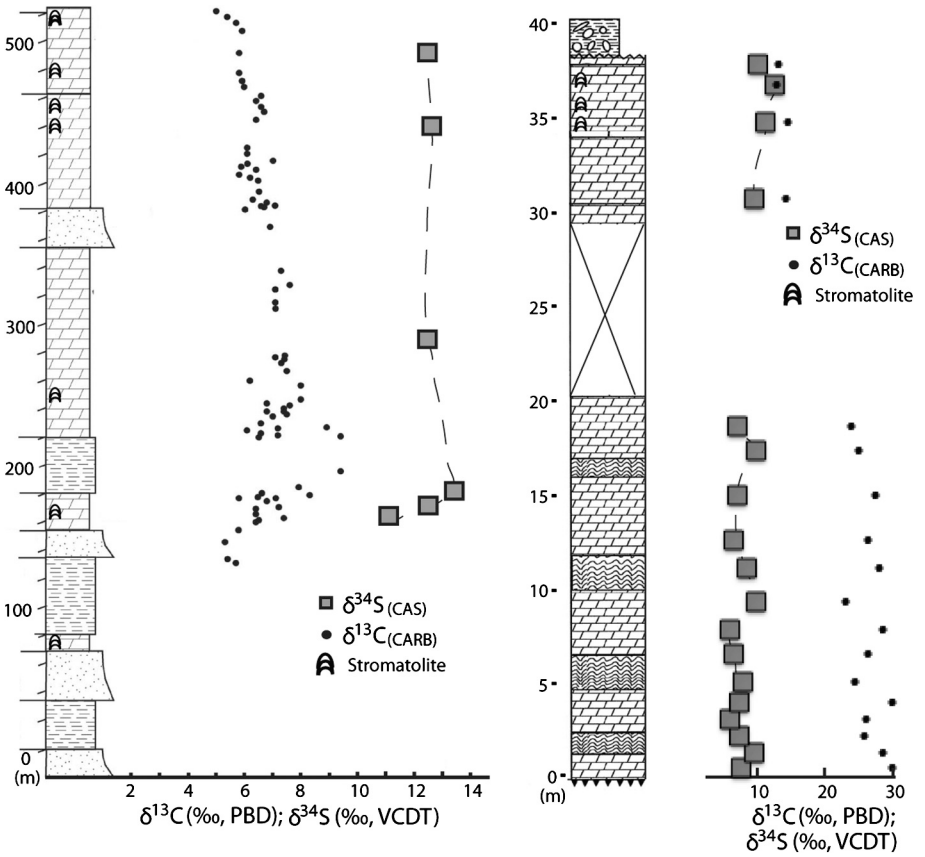

Fig. S5. Carbonate $\delta^{13}C$ and $\delta^{34}S_{CAS}$ stratigraphic trends in the (*A*) Kona Dolomite, United States (modified from ref. 1), and (*B*) Nash Fork Formation, United States (modified from ref. 2).

1 Bekker A, Karhu JA, Kaufman AJ (2006) Carbon isotope record for the onset of the Lomagundi carbon isotope excursion in the Great Lakes area, North America. *Precambrian Res* 148:145–180.

2 Bekker A, Karhu JA, Eriksson KA, Kaufman AJ (2003) Chemostratigraphy of Paleoproterozoic carbonate successions of the Wyoming Craton: Tectonic forcing of biogeochemical change? *Precambrian Res* 120:279–325.

Table S1. Sulfur and carbon data for examined Paleoproterozoic carbonates

Formation/member	Sample name	$\delta^{34}S$ CAS	[CAS]	$\delta^{13}C$ carbonate	$\delta^{18}O$ carbonate	Timing within the LE	Reference on basic geology and correlation
Espanola	EL-2	21.6				Preceding	Bekker et al. (1)
Espanola	El-4	19.7				Preceding	Bekker et al. (1)
Espanola	EL-11	20.3		−2.0	−16.0	Preceding	Bekker et al. (1)
Espanola	EL-34	17.9		−2.0	−14.8	Preceding	Bekker et al. (1)
Espanola	EL-35A	15.0		−2.0	−15.4	Preceding	Bekker et al. (1)
Espanola	EL-39	21.0		−2.1	−13.7	Preceding	Bekker et al. (1)
Espanola	EL-56	29.1		−1.9	−15.7	Preceding	Bekker et al. (1)
Espanola	El-THR-3	15.7				Preceding	Bekker et al. (1)
Kona	MM-30	11.2	121	6.4	−12.4	Early	Bekker et al. (2)
Kona	MM-33	12.7	146	6.4	−12.4	Early	Bekker et al. (2)
Kona	MM-35	13.9		6.4	−11.8	Early	Bekker et al. (2)
Kona	MM-56	12.7		7.1	−12.9	Early	Bekker et al. (2)
Kona	MM-81	12.8		6	−12	Early	Bekker et al. (2
Kona	MM-90	12.7		5.4	−10.9	Early	Bekker et al. (2)
Silverton	Si-5B	12.5	95	9.8	−6.8	Middle	Bekker et al. (3)
Silverton	Si-5A	13.1	70	8.7	−7.9	Middle	Bekker et al. (3)
Silverton	SI-3	13.6	86	9.8	−13.2	Middle	Bekker et al. (3)
Silverton	SI-2/8	14.0		9.74	−8.6	Middle	Bekker et al. (3)
Silverton	SI-2/7	14.9		10.0	−7.0	Middle	Bekker et al. (3)
Silverton	SI-2/14	14.0		10.3	−9.4	Middle	Bekker et al. (3)
Silverton	SI-2-6	11.3		9.4	−9.4	Middle	Bekker et al. (3)
Silverton	Si-2-13	16.0		9.8	−13.2	Middle	Bekker et al. (3)
Lucknow	LK-1	25.8		10.3	−6.7	Middle	Bekker et al. (4); Schröder et al. (5)
Lucknow	LK-2	12.8	274	9.4	−8.0	Middle	Bekker et al. (4); Schröder et al. (5)
Lucknow	LK-3	23.4		10.0	−7.5	Middle	Bekker et al. (4); Schröder et al. (5)
Lucknow	LK-4	26.0		9.7	−6.5	Middle	Bekker et al. (4); Schröder et al. (5)

Formation/member	Sample name	δ^{34}S CAS	[CAS]	δ^{13}C carbonate	δ^{18}O carbonate	Timing within the LE	Reference on basic geology and correlation
Lucknow	LK-9	12.7	393	8.8	−7.4	Middle	Bekker et al. (4); Schröder et al. (5)
Lucknow	Lk-13	25.3	77	10.0	−6.9	Middle	Bekker et al. (4); Schröder et al. (5)
Lucknow	Lk-14	24.5	165	9.5	−6.6	Middle	Bekker et al. (4); Schröder et al. (5)
Nash Fork	BM-1	7.4	151	29.5	−9.2	Middle	Bekker et al. (6)
Nash Fork	BM-2	9.3		28.2	−11.0	Middle	Bekker et al. (6)
Nash Fork	BM-3	6.9	153	25.4	−11.9	Middle	Bekker et al. (6)
Nash Fork	BM-4	5.7	46	25.6	−12.3	Middle	Bekker et al. (6)
Nash Fork	BM-5	7.1	61	29.6	−9.7	Middle	Bekker et al. (6)
Nash Fork	BM-6	7.4	129	24.0	−12.8	Middle	Bekker et al. (6)
Nash Fork	BM-7	6.3	356	25.9	−11.2	Middle	Bekker et al. (6)
Nash Fork	BM-8	5.6		28.1	−9.5	Middle	Bekker et al. (6)
Nash Fork	BM-9	9.6	37	22.7	−10.5	Middle	Bekker et al. (6)
Nash Fork	BM-10	8.2	340	27.5	−10.5	Middle	Bekker et al. (6)
Nash Fork	BM-11	6.2	78	25.9	−11.5	Middle	Bekker et al. (6)
Nash Fork	BM-12	6.8	80	27.1	−10.7	Middle	Bekker et al. (6)
Nash Fork	BM-13	9.5	376	24.7	−11.2	Middle	Bekker et al. (6)
Nash Fork	BM-14	6.8	698	23.5	−11.7	Middle	Bekker et al. (6)
Nash Fork	BM-15	9.1	150	13.9	−10.4	Middle	Bekker et al. (6)
Nash Fork	BM-16	11.0	191	14.3	−12.2	Middle	Bekker et al. (6)
Nash Fork	BM-17	12.2	612	12.6	−13.8	Middle	Bekker et al. (6)
Nash Fork	BM-18	9.7	251	12.9	−13.7	Middle	Bekker et al. (6)
Mcheka	ZA-1	9.5	132	11.1	−6.9	Middle-late	Master et al. (7)
Mcheka	ZA-2	10.2		11.9	−4.6	Middle-late	Master et al. (7)
Mcheka	ZA-3	9.8	111	12.3	−5.6	Middle-late	Master et al. (7)
Mcheka	ZA-4	10.0		11.3	−5.6	Middle-late	Master et al. (7)
Mcheka	ZA-6	11.1	209	11.8	−5.0	Middle-late	Master et al. (7)
Mcheka	ZA-7	11.3	69	10.4	−5.7	Middle-late	Master et al. (7)
Mcheka	ZA-8	11.1	65	11.1	−5.0	Middle-late	Master et al. (7)
Mcheka	ZA-9	11.1	110	11.2	−3.9	Middle-late	Master et al. (7)
Mcheka	ZA-10	11.2	266	11.0	−4.9	Middle-late	Master et al. (7)
Mcheka	ZA-11	11.0	396	11.0	−5.2	Middle-late	Master et al. (7)
Mcheka	ZA-12	10.5	80	10.1	−5.9	Middle-late	Master et al. (7)
Mcheka	ZA-13	10.5	55	10.5	−5.6	Middle-late	Master et al. (7)
Mcheka	ZA-16	11.0	192	10.3	−5.3	Middle-late	Master et al. (7)
Mcheka	ZA-18	11.3	44	9.5	−6.4	Middle-late	Master et al. (7)
Mcheka	ZA-19	10.5	162	10.3	−5.1	Middle-late	Master et al. (7)
Mcheka	ZA-20	13.2	49	10.6	−4.4	Middle-late	Master et al. (7)
Mcheka	ZA-22	12.0	77	10.0	−5.8	Middle-late	Master et al. (7)
Mcheka	ZA-26	11.8	13	9.5	−7.1	Middle-late	Master et al. (7)
Mcheka	ZA-27	11.9	109	10.1	−5.2	Middle-late	Master et al. (7)
Mcheka	ZA-30	14.0	56	9.1	−5.6	Middle-late	Master et al. (7)
Mcheka	ZA-31	16.8	187	9.0	−6.6	Middle-late	Master et al. (7)
Mcheka	ZA-33	12.3	163	8.6	−6.3	Middle-late	Master et al. (7)
Mcheka	ZA-35	12.8	422	8.5	−5.9	Middle-late	Master et al. (7)
Mcheka	ZA-35-2	12.7		8.5	−6.6	Middle-late	Master et al. (7)
Mcheka	ZA-37	15.1	133	8.3	−6.1	Middle-late	Master et al. (7)
Mcheka	Z-3	16.0	49	8.0	−6.5	Middle-late	Master et al. (7)
Mcheka	Z-8	19.1	41	8.1	−5.6	Middle-late	Master et al. (7)
Mcheka	Z-11	15.0	31	8.1	−6.2	Middle-late	Master et al. (7)
Mcheka	Z-13	14.0		7.9	−7.3	Middle-late	Master et al. (7)
Mcheka	Z-15	13.1		8.1	−6.7	Middle-late	Master et al. (7)
Mcheka	Z-16	17.8	31	7.9	−6.6	Middle-late	Master et al. (7)
Mcheka	Z-19	17.8		8.0	−6.8	Middle-late	Master et al. (7)
Mcheka	Z-2	16.3	33	7.8	−6.6	Middle-late	Master et al. (7)
Mcheka	Z-20	19.0		7.9	−6.8	Middle-late	Master et al. (7)
Mcheka	Z-21	16.7	27	8.3	−5.8	Middle-late	Master et al. (7)
Mcheka	Z-25	17.6	28	7.6	−7.3	Middle-late	Master et al. (7)
Mcheka	Z-26	13.7	16	7.7	−6.7	Middle-late	Master et al. (7)
Mcheka	SLD-9	14.6		9.5	−7.6	Middle-late	Master et al. (7)
Mcheka	SLD-14-1	9.4		11.1	−6.3	Middle-late	Master et al. (7)
Mcheka	SLD-14-2	9.4	302	11.1	−6.3	Middle-late	Master et al. (7)
Mcheka	SLD-15	8.2		11.8	−6.1	Middle-late	Master et al. (7)
Mcheka	SLD-20	8.8		11.4	−6	Middle-late	Master et al. (7)
Mcheka	SLD-21	9.3		11.8	−5.9	Middle-late	Master et al. (7)
Mcheka	SLD-24	12.4		11.7	−4.7	Middle-late	Master et al. (7)
Mcheka	SLD-28	12.6		10.9	−5.7	Middle-late	Master et al. (7)
Mcheka	SLD-32	10.8		10.6	−5.2	Middle-late	Master et al. (7)
Mcheka	SLD-35	12.9		9.6	−6.7	Middle-late	Master et al. (7)
Mcheka	SLD-38	12.1		10.0	−5.3	Middle-late	Master et al. (7)
Mcheka	NJ-6	16.6		7.1	−9.9	Middle-late	Master et al. (7)
Lower Albanel	MI-18-2	27.7	32	4.8	−8.5	Late	Bekker et al. (6)

Formation/member	Sample name	δ^{34}S CAS	[CAS]	δ^{13}C carbonate	δ^{18}O carbonate	Timing within the LE	Reference on basic geology and correlation
Lower Albanel	MI-16-5	30.9		5.4	−7.9	Late	Bekker et al. (6)
Lower Albanel	MI-16-2	28.3		5.3	−8.7	Late	Bekker et al. (6)
Lower Albanel	MI-14-66	28.8				Late	Bekker et al. (6)
Lower Albanel	MI-18-4	19.4		1.0	−8.1	Post	Bekker et al. (6)
Lower Albanel	LA-2	18.1	29	1.1	−4.9	Post	Bekker et al. (6)
Lower Albanel	LAF-F3	46.6	37	1.5	−4.4	Post	Bekker et al. (6)
Lower Albanel	UAF-2		42	2.1	−6.5	Post	Bekker et al. (6)
Lower Albanel	UAF-1	42.0	52	2.2	−6.5	Post	Bekker et al. (6)
Lower Albanel	LA-E4	37.1	39	1.1	−3.0	Post	Bekker et al. (6)
Lower Albanel	LAF-4	43.0	66	−0.9	−11.0	Post	Bekker et al. (6)
Lower Albanel	LA-D5	30.1	48	2.4	−3.4	Post	Bekker et al. (6)
Lower Albanel	LAF-D2	31.3	67	2.8	−3.2	Post	Bekker et al. (6)

1 Bekker A, Kaufman AJ, Karhu JA, Eriksson KA (2005) Evidence for Paleoproterozoic cap carbonates in North America. *Precambrian Res* 137:167–206.
2 Bekker A, Karhu JA, Kaufman AJ (2006) Carbon isotope record for the onset of the Lomagundi carbon isotope excursion in the Great Lakes area. *Precambrian Res* 148:145–180.
3 Bekker A, et al. (2008) Fractionation between inorganic and organic carbon during the Lomagundi (2.22–2.1 Ga) carbon isotope excursion. *Earth Planet Sci Lett* 271:278–291.
4 Bekker A, et al. (2001) Chemostratigraphy of the Paleoproterozoic Duitschland Formation, South Africa: Implications for coupled climate change and carbon cycling. *Am J Sci* 301:261–285.
5 Schröder S, Bekker A, Beukes NJ, Strauss H, vanNiekerk HS (2008) Rise in seawater sulphate concentration associated with the Paleoproterozoic positive carbon isotope excursion: Evidence from sulphate evaporites in the similar to 2.2–2.1 Gyr shallow-marine Lucknow Formation, South Africa. *Terra Nova* 20:108–117.
6 Bekker A, Eriksson KA (2003) A Paleoproterozoic drowned carbonate platform on the southeastern margin of the Wyoming Craton: A record of the Kenorland breakup. *Precambrian Res* 120: 327–364.
7 Master S, Bekker A, Hofmann A (2010) A review of the stratigraphy and geological setting of the Palaeoproterozoic Magondi Supergroup, Zimbabwe–Type locality for the Lomagundi carbon isotope excursion. *Precambrian Res* 182:254–273.
8 Bekker A, Karhu JA, Eriksson KA, Kaufman AJ (2003) Chemostratigraphy of Paleoproterozoic carbonate successions of the Wyoming Craton: Tectonic forcing of biogeochemical change? *Precambrian Res* 120: 279–325.

Table S2. Proterozoic and Paleozoic CAS concentrations

Age	Average [CAS] (ppm)	1σ (ppm)	Location	Reference
Late Cambrian	299	164	North Australia, central USA	Gill et al. (1)
Mid-Neoproterozoic	65	66	South Australia, Namibia, southwestern USA	Hurtgen et al. (2)
Mid-Mesoproterozoic, late Paleoproterozoic	20	9	North Australia, central USA	Gellatly et al. (3)
Mid-Mesoproterozoic, late Paleoproterozoic	143	100	North China	Chu et al. (4)
Mid-Paleoproterozoic, (final stages and the aftermath of the LE)	48	12	Mistassini Basin, eastern Canada	This study
Mid-Paleoproterozoic, (middle to end of the LE)	117	110	Upper part of Mcheka Formation, Zimbabwe	This study
Mid-Paleoproterozoic (middle part of the LE)	227	137	Lucknow Formation, South Africa	This study
Mid-Paleoproterozoic, (middle part of the LE)	232	198	Nash Fork Formation, western USA	This study
Early to mid-Paleoproterozoic (all)	150	145	Central and western USA, Zimbabwe, eastern Canada, South Africa	This study

1 Gill BC, et al. (2011) Geochemical evidence for widespread euxinia in the Later Cambrian ocean. *Nature* 469:80–83.
2 Hurtgen MT, Arthur MA, Halverson GP (2005) Neoproterozoic sulfur isotopes, the evolution of microbial sulfur species, and the burial efficiency of sulfide as sedimentary pyrite. *Geology* 33:41–44.
3 Gellatly AM, Lyons TW (2005) Trace sulfate in mid-Proterozoic carbonates and the sulfur isotope record of biospheric evolution. *Geochim Cosmochim Acta* 69:3813–3829.
4 Chu XL, Zhang TG, Zhang QR, Lyons TW (2007) Sulfur and carbon isotope records from 1700 to 800 Ma carbonates of the Jixian section, northern China: Implications for secular isotope variations in Proterozoic seawater and relationships to global supercontinental events. *Geochim Cosmochim Acta* 71:4668–4692.

Table S3. Estimates of marine sulfate concentrations through time

Eon/era	Age (Myr)	Estimate of marine [sulfate] (mM)	Basis for estimate	Reference
Phanerozoic	542–0	*ca*. 5–30	Direct measurement of [sulfate] from fluid inclusions	Lowenstein et al. (1); Horita et al. (2); Brennan et al. (3)
Paleozoic	542–251	*ca*. 5–30	Extent of CAS isotopic variability during positive carbon isotope excursions	Gill et al. (4)
Proterozoic	1,650–630	*ca*. 1–7	Extent of CAS isotopic variability in thick carbonate successions	Kah et al. (5)
Proterozoic	2,100; 1,300; 1,200; 800	>2.5	Presence of thick sulfate evaporate successions and precipitation of sulfate before halite during the evaporation sequences	Schröder et al. (6)
Paleoproterozoic	2,100; 2,250	*ca*. 5–20	Extent of CAS isotopic variability during the falling limb of the Lomagundi positive carbon isotope excursion	This study

Eon/era	Age (Myr)	Estimate of marine [sulfate] (mM)	Basis for estimate	Reference
Mid-Proterozoic	18,00–700	<1	Maximum sulfur isotope fractionation during bacterial sulfate reduction based on the temporal isotopic record of pyrite and sulfate	Canfield et al. (7)
Archean	3,800–2,500	<0.2	Maximum sulfur isotope fractionation during bacterial sulfate reduction based on the temporal isotopic record of pyrite and sulfate	Habicht et al. (8)

1 Lowenstein TK, Timofeeff MN, Brennan ST, Hardie LA, Demicco RV (2001) Oscillations in Phanerozoic seawater chemistry: Evidence from fluid inclusions. *Science* 294:1086–1088.
2 Horita J, Zimmermann H, Holland HD (2002) Chemical evolution of seawater during the Phanerozoic: Implications from the record of marine evaporites. *Geochim Cosmochim Acta* 66:3733–3756.
3 Brennan ST, Lowenstein TK, Horita J (2004) Seawater chemistry and the advent of biocalcification. *Geology* 32:473–476.
4 Gill BC, Lyons TW, Saltzman MR (2007) Parallel, high-resolution carbon and sulfur isotope records of the evolving Paleozoic marine sulfur reservoir. *Palaeogeogr Palaeoclimatol Palaeoecol* 256:156–173.
5 Kah LC, Lyons TW, Frank T (2004) Low marine sulphate and protracted oxygenation of the Proterozoic biosphere. *Nature* 431:834–837.
6 Schröder S, Bekker A, Beukes NJ, Strauss H, van Niekerk HS (2008) Rise in seawater sulphate concentration associated with the Paleoproterozoic positive carbon isotope excursion: Evidence from sulphate evaporites in the similar to 2.2–2.1 Gyr shallow-marine Lucknow Formation, South Africa. *Terra Nova* 20:108–117.
7 Canfield DE, Farquhar J, Zerkle AL (2010) High isotope fractionations during sulfate reduction in a low-sulfate euxinic ocean analog. *Geology* 38:415–418.
8 Habicht KS, Gade M, Thamdrup B, Berg P, Canfield DE (2002) Calibration of sulfate levels in the Archean Ocean. *Science* 298:2372–2374.

Table S4. Sulfur isotope data from evaporites deposited during the Lomagundi excursion

Name of unit (location)	Age (Ga)	Type of evaporite	$\delta^{13}C$ (‰)	$\delta^{34}S$ (‰)	Reference
Gordon Lake Formation, Huronian Supergroup (Lake Huron, Canada)	*ca*. 2.3–2.22	Silicified and pristine anhydrite and gypsum nodules and layers	5.0–8.2	11.7–15.6	Cameron (1), Chandler (2), Bennett et al. (3), Bekker et al. (4)
Kona Dolomite, Chocolay Group (Michigan, USA)	*ca*. 2.3–2.22	Pseudomorphs after gypsum and anhydrite	5.0–9.5	11.4–16.0	Bekker et al. (4), Taylor (5), Clark (6), Wohlabaugh (7), Hemzacek et al. (8), Hemzacek (9), Perry et al. (10), Feng (11), Genest (12)
Lower Umba Formation, Lower Jatulian Group (Imandra–Varzuga Belt, Kola Peninsula, Russia)	*ca*. 2.2	Barite beds	2.3–6.7	27.8–34.2	Melezhik and Fetisova (13), Grinenko et al. (14), Melezhik and Fallick (15)
Lucknow Formation, Postmasburg Group (South Africa)	*ca*. 2.15	Molds and quartz pseudomorphs after gypsum and anhydrite	8.4–11.3	9.2–14.0	Master et al. (16), Swart (17), Schröder et al. (18)
Delwara Formation and Jhamarkotra Formation, Aravalli Group (Rajasthan, India)	*ca*. 2.1	Barite layers	5.1–11.1	17.1–21.2	Deb et al. (19), Sreenivas et al. (20)
Fedorovka Formation (Aldan Shield, Siberia, Russia)	*ca*. 2.1	Anhydrite layers and veins	−1.7–5.5	up to 32.1	Zolotarev et al. (21), Velikoslavinsky et al. (22), Guliy and Wada (23)

Table after Bekker et al. (4) and Schröder et al. (16).

1 Cameron EM (1983) Evidence from early Proterozoic anhydrite for sulfur isotopic partitioning in Precambrian oceans. *Nature* 304:54–56.
2 Chandler FW (1988) Diagenesis of sabkha related, sulphate nodules in the Early Proterozoic Gordon Lake Formation, Ontario, Canada. *Carbonates Evaporites* 3:75–94.
3 Bennett G, Born P, Hatfield K (1989) A report on a recently identified dolostone unit in Fenwick Township, Goulais Bay area, District of Algoma. *Ont Geol Surv Misc Pap* 142:211–215.
4 Bekker A, Karhu JA, Kaufman AJ (2006) Carbon isotope record for the onset of the Lomagundi carbon isotope excursion in the Great Lakes area, North America. *Precambrian Res* 148:145–180.
5 Taylor GL (1972) Stratigraphy, sedimentology, and sulfide mineralization of the Kona Dolomite. PhD dissertation (Michigan Technological Institute, Lansing, MI).
6 Clark JL (1974) Sulfide mineralization in the Kona Dolomite, Marquette County, Michigan. Master's thesis (Michigan Technological University, Houghton, MI).
7 Wohlabaugh N (1980) *Petrology of the Big Cusp Algal Dolomite; An Informal Member of the Kona Dolomite*. (Michigan Bowling Green State University, Marquette).
8 Hemzacek JM, Perry EC, Larue DK, Feng J (1982) Sulfur isotope composition of sulfate in chert horizons of the Proterozoic (Precambrian X) Kona Dolomite, Marquette Region, Michigan. *Geol Soc Am Abstr* 14:512.
9 Hemzacek JM (1987) Replaced evaporites and the sulfur isotope age curve of the Precambrian. Master's thesis (Northern Illinois University, DeKalb, IL).
10 Perry EC, Feng J, Hemzacek JM (1984) Precambrian evaporites: Preservation of sulfate in quartz pseudomorphs after gypsum. *Proc Inst Lake Superior Geol* 30:47.
11 Feng J (1986) Sulfur and oxygen isotope geochemistry of Precambrian marine sulfate and chert. Master's thesis (Northern Illinois University, DeKalb, IL).
12 Genest S (1985) Aphebian evaporites and related red beds in the Peribonca Formation (Otish Group, Central Quebec): Evidence for coastal sabkha and subaqueous environments. *GAC-MAC Programs Abstr* 10:A21.
13 Melezhik VA, Fetisova OA (1989) First discovery of syngenetic barites in the Precambrian of the Baltic Shield. *Doklady Akademii Nauk* 307:422–425.
14 Grinenko LN, Melezhik VA, Fetisova OA (1989) First discovery of barites in the Precambrian sedimentary deposits of Baltic Shield. *Dokl Akad Nauk* 304:1453–1455.
15 Melezhik VA, Fallick AE (1996) A widespread positive $\delta^{13}C$ carb anomaly at around 2.33–2.06 Ga on the Fennoscandian Shield: A paradox? *Terra Nova* 8:141–157.
16 Master S, Verhagen BT, Bassot JP, Beukes NJ, Lemoine S (1993) Stable isotopic signatures of Paleoproterozoic carbonates from Guinea, Senegal, South Africa and Zimbabwe: Constraints on the timing of the *ca*. 2 Ga Lomagundi $\delta^{13}C$ excursion. *Proceedings of the International Symposium Early Proterozoic, Geochemical and Structural Constraints—Metallogeny*, ed Abdoulaye DIA (Centre International pour la Formation et les Echanges Geologiques, Dakar), pp 38–41.
17 Swart QD (1999) Carbonate rocks of the Paleoproterozoic Pretoria and Postmasburg Groups, Transvaal Supergroup. Master's thesis (Rand Afrikaans University, Johannesburg).
18 Schröder S, Bekker A, Beukes, NJ, Strauss H, van Niekerk, HS (2008) Rise in seawater sulphate concentration associated with the Paleoproterozoic positive carbon isotope excursion: evidence from sulphate evaporites in the similar to 2.2–2.1 Gyr shallow-marine Lucknow Formation, South Africa. *Terra Nova* 20:108–117.
19 Deb M, Hoefs J, Baumann A (1991) Isotopic composition of two Precambrian stratiform barite deposits from the Indian shield. *Geochim Cosmochim Acta* 55:303–308.
20 Sreenivas B, et al. (2001) Positive $\delta^{13}C$ excursion in carbonate and organic fractions from the Paleoproterozoic Aravalli Supergroup, Northwestern India. *Precambrian Res* 106:277–290.
21 Zolotarev AA, Efremov GM, Brotigam B, Ivanova TV (1989) Isotopic composition of sulfur in sulfates of Seligdar apatite deposit (Central Aldan). *Geokhimiya* 11:1656–1659.
22 Velikoslavinsky SD, et al. (2003) The U–Pb age of the Fedorov Sequence of the Aldan granulite—gneiss megacomplex, the Aldan Shield. *Dokl Earth Sci* 393:1151–1155.
23 Guliy VN, Wada H (2003) Macro- and microvariations of isotopic composition of carbon and oxygen of carbonates from the Precambrian of the Aldan Shield. *Geokhimiya* 5:482–491.